Study of Stress Birefringence for 193-nm Immersion Photomasks

Eric Cotte[a]*, Michael Selle[b], Karsten Bubke[a], and Silvio Teuber[a]
[a]Advanced Mask Technology Center (AMTC), Technology Development Dept.,
Rähnitzer Allee 9, 01109 Dresden (Germany)
[b]SCHOTT Lithotec AG, Göschwitzer Str. 20, 07745 Jena (Germany)

ABSTRACT

The goal of the present study was to investigate and quantify reticle stress birefringence in exposure conditions. Birefringence can arise in fused silica photomask substrates due to their state of stress, and cause optical effects such as phase front distortion, ray bifurcation, and polarization changes. These effects potentially produce image blurring and illumination non-uniformity, leading to lower resolution and CD variations, respectively. The main sources of substrate stress studied were the absorber stack, the mounting of a pellicle, and the impact of initial reticle bow when chucking in an exposure tool. Jones calculus was used to relate birefringence at discrete locations in the reticle, derived from the state of stress, to the net birefringence experienced by light passing through the mask. Experimentally-obtained birefringence data as well as analytical calculations of stress birefringence caused by known states of stress were used to validate the models. These results can then be compared to photomask birefringence specifications or employed in optical simulations to determine the precise impact of this substrate stress birefringence.

Keywords: birefringence, stress, photomask, Jones calculus.

1. INTRODUCTION

As the latest ITRS report illustrates, the semiconductor industry could rely on optical lithography and transmissive masks down to the 45-nm node.[1] At such design rules, sources of optical distortions such as birefringence need to be closely monitored. In particular, specifications on maximum allowable photomask birefringence will be set, related to projection system lens designs, and are expected to be in the range of a few nm/cm.

Stress in the mask substrate generates variations in indices of refraction (referred to as birefringence when the index of refraction is different for two perpendicular directions), which in turn induce phase distortions, causing printing errors. This photoelastic effect, producing an anisotropic optical behavior, is called stress birefringence. For substrates, residual birefringence refers to the stress birefringence that comes from internal stresses in the substrate due to its fabrication and processing. In this paper, all external sources of stress (i.e., except residual stresses from substrate fabrication) were taken into account in the finite element (FE) models, as they could suffice to generate large birefringence, although some of these sources of stress were negligible when considering causes of reticle in-plane displacements.[2-5]

More precisely, the focus was placed on substrate bow (currently ranging from 0.5 µm to 1.0 µm), Cr layer stress and thickness, pellicle type (dimensions and gasket compliance) and pellicle frame bow, as well as exposure tool chucking area and vacuum chucking pressure. Section 2 explains how equations were derived to calculate the net birefringence through the mask (along the path of light traversing the reticle) from the birefringence readily determined on various surfaces of the mask, using Jones calculus. Verification of the simulations was performed via an analytical test case and experiments mimicking the reticle loads and boundary conditions in an exposure tool, as shown in Sections 3 and 4. The birefringence changes were tracked as the loadings were modified, and the experimental data was compared to the numerical prediction to validate the models. Thus, stress birefringence for a reticle held in an exposure tool were quantified.

*email: Eric.Cotte@amtc-dresden.com

2. ASSESSING MASK STRESS BIREFRINGENCE

The calculations necessary for the determination of stress birefringence are outlined in Fig. 1. The method implemented in this article is similar to that described in publications by Genberg and Doyle.[6-10] Basically, an FE software is used to simulate the state of stress in the substrate from its loading. From the principal stresses, birefringence is evaluated at given cross-sections. Finally, using representation by Jones matrices and solving the eigenproblem, net birefringence is calculated.

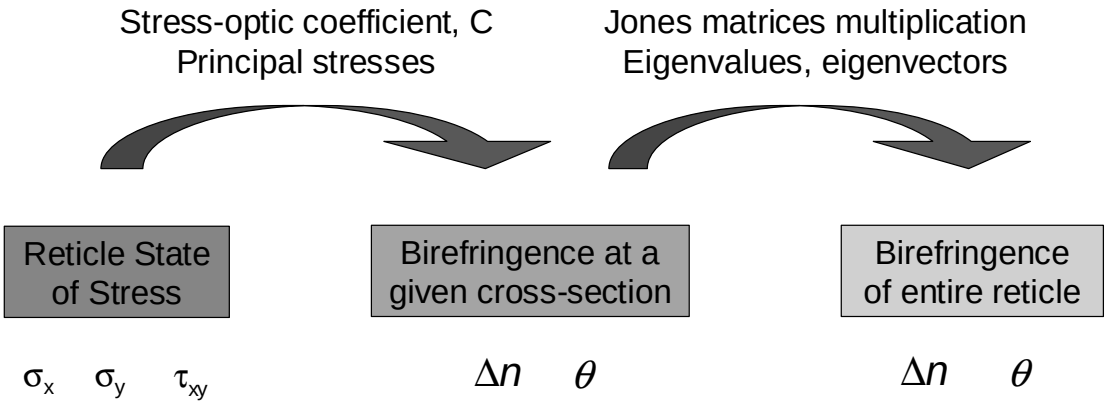

Fig. 1. Flow chart of birefringence calculation method.

As already mentioned, the loadings include deposition of stressed layers, pellicle attachment, and vacuum chucking of a mask with a bowed substrate. The substrate is treated as a thin plate in plane stress, which is characterized by stresses σ_x and σ_y, as well as a shear stress τ_{xy}. The principal stresses σ_1 and σ_2, as well as their orientation, represented by the angle θ, are calculated, using Eqs. (1) through (3). Notations are illustrated in Fig. 2, and Fig. 2 (c) provides a graphical representation of the state of stress, as a Mohr's circle, i.e., a plot of shear stress as a function of stress.

$$\sigma_1 = \frac{\sigma_x + \sigma_y}{2} + \sqrt{\left(\frac{\sigma_x - \sigma_y}{2}\right)^2 + \tau_{xy}^{\,2}}\,,\quad \sigma_2 = \frac{\sigma_x + \sigma_y}{2} - \sqrt{\left(\frac{\sigma_x - \sigma_y}{2}\right)^2 + \tau_{xy}^{\,2}}\,,\quad \tan 2\theta = \frac{2\tau_{xy}}{\sigma_x - \sigma_y} \qquad (1), (2), (3)$$

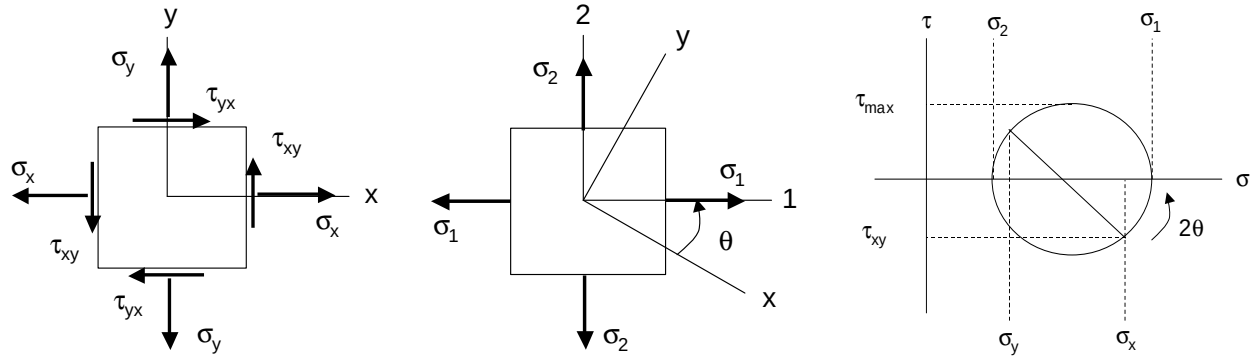

(a) (b) (c)

Fig. 2. (a) Stresses in the Cartesian coordinate system, (b) principal stresses, and (c) Mohr's circle.[11]

Subsequently, the stress birefringence at each point of an isotropic material can be calculated using a relation linking the dielectric impermeability tensor to the state of stress via the stress-optic coefficients of the substrate material:[12]

$$(\Delta\beta) = \begin{pmatrix} q_{11} & q_{12} & q_{12} & 0 & 0 & 0 \\ q_{12} & q_{11} & q_{12} & 0 & 0 & 0 \\ q_{12} & q_{12} & q_{11} & 0 & 0 & 0 \\ 0 & 0 & 0 & q_{44} & 0 & 0 \\ 0 & 0 & 0 & 0 & q_{44} & 0 \\ 0 & 0 & 0 & 0 & 0 & q_{44} \end{pmatrix} (\sigma), \text{ with } q_{44} = \frac{q_{11} - q_{12}}{2} \tag{4}$$

The changes in refraction index in the principal directions are related to the dielectric impermeability by:

$$\Delta n_1 = -\frac{1}{2} n^3 \Delta\beta_1 \qquad \text{and} \qquad \Delta n_2 = -\frac{1}{2} n^3 \Delta\beta_2 . \tag{5), (6}$$

Equations (4) through (6) thus yield the formulas derived by Yiu and Meyer:[13]

$$\Delta n_1 = -\frac{1}{2} n^3 (q_{11} \times \sigma_1 + q_{12} \times \sigma_2 + q_{12} \times \sigma_3), \tag{7}$$

$$\Delta n_2 = -\frac{1}{2} n^3 (q_{12} \times \sigma_1 + q_{11} \times \sigma_2 + q_{12} \times \sigma_3). \tag{8}$$

After simplification, the birefringence $\Delta n_{1\text{-}2} = \Delta n_1 - \Delta n_2$ can be linked to the state of stress and a single stress-optic coefficient, denoted as C, with a single equation:

$$\Delta n_{1\text{–}2} = -\frac{1}{2} n^3 (q_{11} - q_{12}) \times (\sigma_1 - \sigma_2) = \mathrm{C} \times (\sigma_1 - \sigma_2). \tag{9}$$

Birefringence is not only characterized by its magnitude, Δn, but also by directions called the fast axis, which is the same as the first principal direction, and the slow axis. This birefringence pertains to a single point in the medium, and a collection of such points at a given cross-section can yield a birefringence map. Yet, such a map is not representative of the birefringence experienced by a ray crossing the substrate, but only of the birefringence at that cross-section. As illustrated in Fig. 1, the net birefringence of a substrate must be obtained using the values of birefringence and fast axes at all cross-sections of the medium, via Jones calculus.

A polarization-inducing medium such as a substrate with a fast axis rotated by an angle θ with respect to the x axis can be represented, via Jones calculus, as an arbitrarily-oriented retarder $M(\theta)$, i.e., the product of a linear retarder oriented along the x and y axes, with a retardation defined as $\delta = \delta_x - \delta_y$, M, and a rotation matrix $R(\theta)$:

$$M(\theta) = R(\theta) \times M \times R(-\theta), \tag{10}$$

with

$$R(\theta) = \begin{pmatrix} \cos\theta & -\sin\theta \\ \sin\theta & \cos\theta \end{pmatrix}, \tag{11}$$

and $M = \begin{pmatrix} e^{i\delta_x} & 0 \\ 0 & e^{i\delta_y} \end{pmatrix} = e^{i(\frac{\delta_x}{2}+\frac{\delta_y}{2})} \begin{pmatrix} e^{i\frac{\delta}{2}} & 0 \\ 0 & e^{-i\frac{\delta}{2}} \end{pmatrix}$, or, neglecting a phase offset , $M = \begin{pmatrix} e^{i\frac{\delta}{2}} & 0 \\ 0 & e^{-i\frac{\delta}{2}} \end{pmatrix}$. (12)

Thus, for light with a wavelength λ, an arbitrarily-oriented retarder of thickness t with retardance $\delta = \frac{2\pi t}{\lambda}\Delta n_{1-2}$ can be written as the following Jones matrix:

$$M(\theta) = \begin{pmatrix} \cos^2\theta \times e^{i\frac{\delta}{2}} + \sin^2\theta \times e^{-i\frac{\delta}{2}} & 2i \times \sin\theta \times \cos\theta \times \sin\left(\frac{\delta}{2}\right) \\ 2i \times \sin\theta \times \cos\theta \times \sin\left(\frac{\delta}{2}\right) & \sin^2\theta \times e^{i\frac{\delta}{2}} + \cos^2\theta \times e^{-i\frac{\delta}{2}} \end{pmatrix}. \quad (13)$$

A property of this matrix is that its eigenvalues yield the magnitude of the birefringence of the medium, while the fast axis can be obtained from its eigenvectors. Such a matrix also permits to determine the state of an outcoming ray, represented by its Jones vector *J'* as a function of an incoming ray, represented by its Jones vector *J*, as shown in Fig. 3 (a). In the case of multiple media, as depicted in Fig 3 (b), the Jones matrix for the group is calculated as the product of the Jones matrices of its elements. For example, for 3 different media:

$$J' = M_3(\theta_3) \times M_2(\theta_2) \times M_1(\theta_1) \times J \quad (14)$$

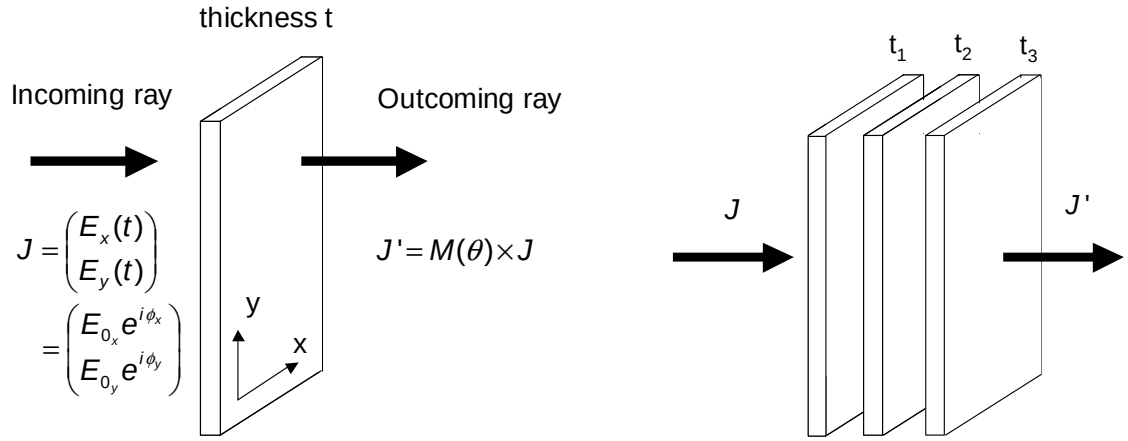

Fig. 3. Jones calculus for (a) one medium and (b) multiple media, via Eq. (14).

Thus, and since finite element models are already discretized, this approach of multiplying the Jones matrices of many media can be used to form a Jones matrix representing the optical behavior of the entire thickness of the substrate from data gathered at the model's nodes. Finally, having formed this Jones matrix representing the whole mask thickness, it is possible to extract the equivalent net birefringence of the mask by solving for its eigenvalues (to calculate the magnitude of the birefringence Δn) and its eigenvectors (to obtain the fast axis angle θ) of the full substrate's Jones matrix.

3. ANALYTICAL TEST CASE

As an example, birefringence was calculated analytically for a particular mask loading: the bending loads, which are the main loads experienced by the mask during its exposure and thus the most probable potential sources of stress birefringence. The case of a plate subjected to uniaxial bending was considered: a square plate is supported along 2 opposite edges and loaded uniformly along its centre, as shown on Fig. 4. Figure 4 (b) also features the stress profile through the thickness of the substrate for uniaxial bending.

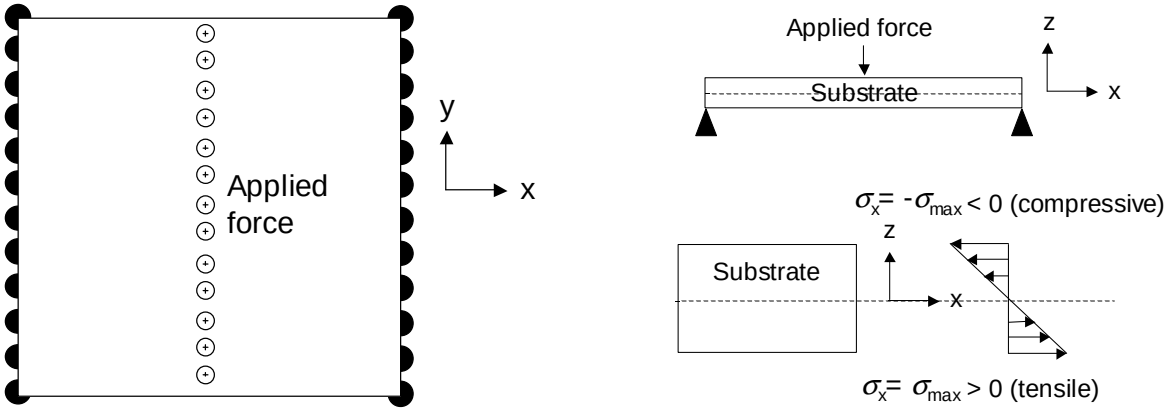

Fig. 4. Plate in state of uniaxial bending: (a) top view and (b) side view and resulting stress profile.

Analytically, the stress at a given location (x,y) and through the thickness of the blank is such that it varies linearly with the z-location: it reaches a value $\sigma_{max}(x)$, written simply as σ_{max} in the figures, on the bottom surface and $-\sigma_{max}(x)$ on the top surface, while it is null at the middle surface of the plate (also called neutral surface for that reason). Thus, the state of stress can easily be described at any point of the blank. From these data, principal stresses σ_1 and σ_2 can be calculated, and therefore birefringence at given cross-sections can be determined (both magnitude and direction), via the material's stress-optic coefficient C as illustrated in Fig. 5.

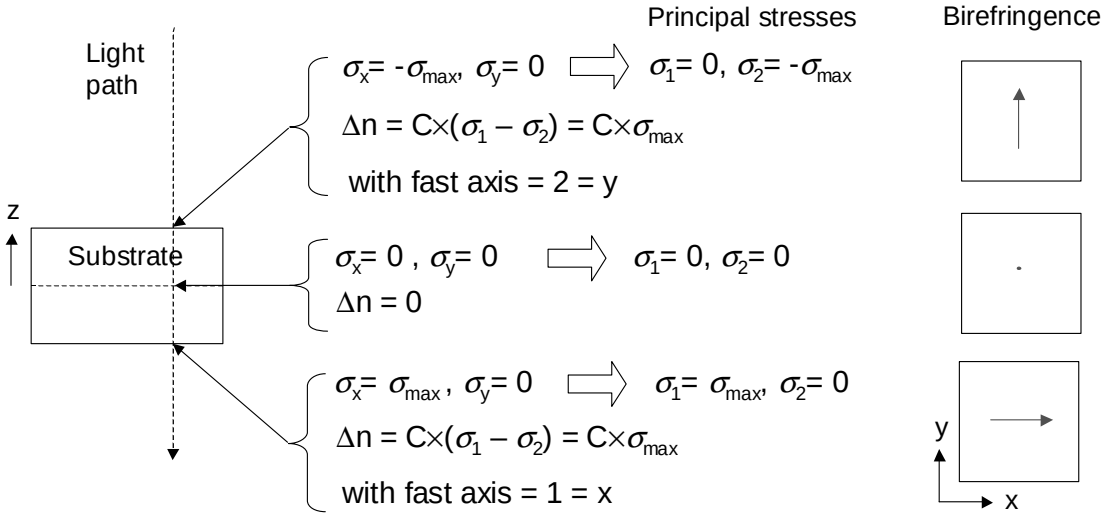

Fig. 5. Calculation of stresses, principal stresses, and birefringence at different locations of a blank loaded as in Fig. (4).

The birefringence on the neutral surface of the substrate is therefore null, due to the stress being null. The magnitude of the birefringence is $C \times \sigma_{max}(x)$ both at the top and bottom of the substrate, but the fast axes do not coincide: they are perpendicular. To obtain the birefringence along the light path through the substrate, a Jones matrix representing the net state of birefringence must be created and multiplied. The eigenvalues of the product matrix yield the net, or 'integrated', birefringence through the substrate. Although this appears to be a complex and involved calculation, simple observations on the multiplication of Jones matrices and optical laws provide a quick answer. Indeed, as shown on Fig. 5, the states of birefringence at two points on either side of the neutral axis are perpendicular, which makes the net polarizing effect on light going through these two points null. Applying the same argument for all points on either side on the neutral axis, and since the birefringence is null on the neutral axis, the net birefringence is null, i.e., a substrate in a state of uniaxial bending has no stress birefringence.

4. NUMERICAL APPLICATION OF METHOD AND EXPERIMENTAL VERIFICATION

A finite element simulation was run, replicating the loading considered in Section 3, and the model correctly predicted that no stress birefringence arises from this uniaxial bending type of loading. Then, a model with reticle loadings corresponding to those of a mask vacuum-chucked in an exposure tool was created, incorporating the influence of a stressed absorber layer, variable vacuum-chucking areas and pressures, pellicle attachment, as well as an initial substrate shape. Figure 6 depicts the loads on the reticle from vacuum chucking and, in particular, Figs. 6 (b) and (c) illustrate the smallest and largest chucking areas modeled in order to cover various exposure tools. A value of substrate stress-optic coefficient $C = 5.25 \times 10^{-5}$ nm/cm/Pa was used for a wavelength of 193 nm.[14] The modeling of pellicle attachment on mask image placement and its verification was explained in a past publication.[15] The initial substrate shapes modeled were axisymmetric and similar to shapes induced by a stressed absorber as described by Stoney's equation, as shown in Fig. 7.[16]

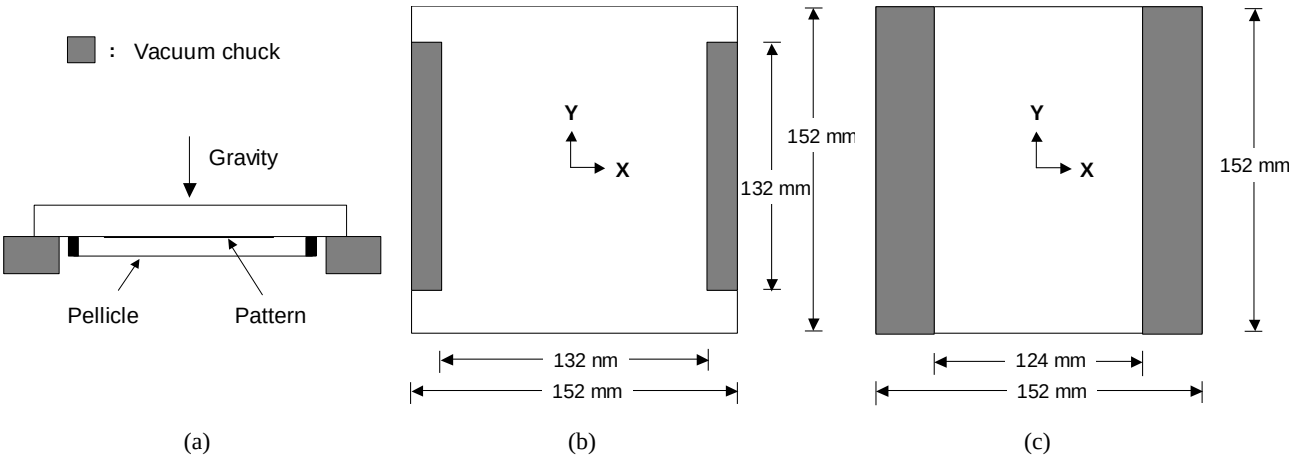

Fig. 6. Schematics of a mask held in an exposure tool vacuum-chuck: (a) side-view, and top view for the case of (b) the smallest and (c) the largest chucking area considered.

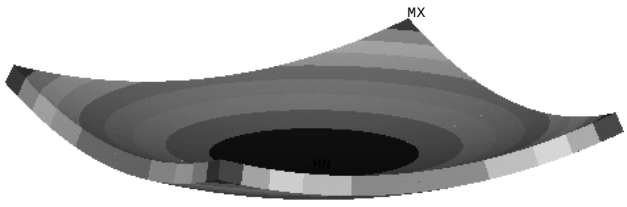

Fig. 7. Example of a substrate shape due to the deposition of a uniformly stressed layer.

Simulations showed that the stress birefringence was small, below 1 nm/cm, for a typical case as well as cases run with various combinations of substrate initial shape, absorber layer stress, attached pellicle, chucking pressure, and chucking area size. A possible explanation why stress birefringence is so small is that the state of stress is mostly bending, even though it is not uniaxial bending as in the example in Section 3. To verify these results, an experiment was set up, as described in Fig. 8, to measure the birefringence of a blank subjected to a loading approaching the mounting conditions in an exposure tool, i.e., similar to the cases modeled.

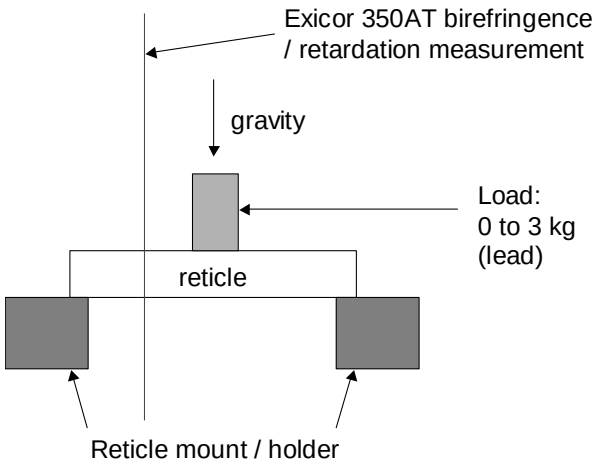

Fig. 8. Side view of a schematic of the experimental setup, featuring a reticle, reticle holder, and lead load.

The experiment was run at Schott Lithotec, using an Exicor 350 AT tool from Hinds instruments.[17-19] The blank was held horizontally, supported along 2 opposite edges, and a variable load was applied in its centre to replicate the contribution of gravity acting on a mask in an exposure tool. A load of up to 3 kg was applied, corresponding to a loading larger than that provided by gravity, to magnify the potential stress birefringence effects and be certain to capture them. Birefringence was measured for various loads to monitor possible changes and compare results to modeling predictions. Figures 9 through 11 show selected results of the experiment for a substrate subjected to gravity only, to gravity and a mass of 3 kg, and again for gravity only (to check repeatability), respectively. In Fig. 10, the absence of data in a rectangle near the center of the substrate is simply due to the presence of the lead load.

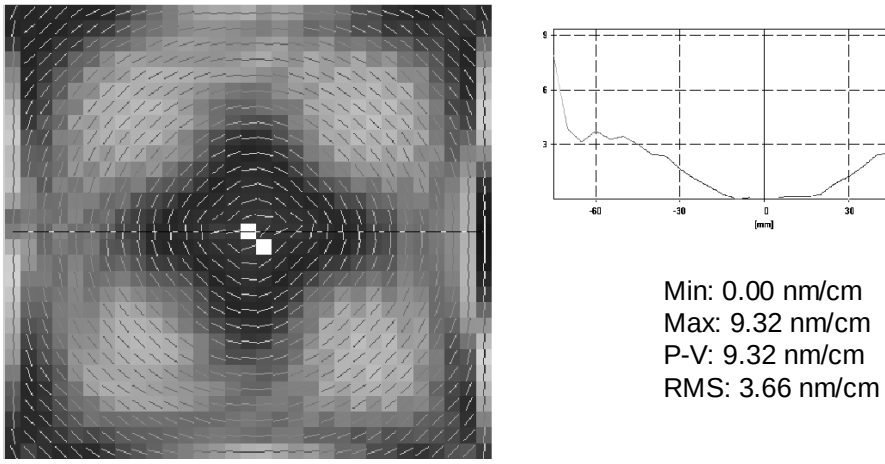

Fig. 9. Experimentally measured birefringence for a substrate under gravity, without any additional load.

In Figs. 9 through 11, the mask area monitored is not square, but slightly rectangular, as the extreme top and bottom parts of the substrate cannot be measured: they correspond to the edges along which the substrate is supported. Nevertheless, it can be observed, by comparing the results in Figs. 10 and 11, that the state of birefringence with a 3 kg load is roughly the same as with gravity only, i.e., it is equal to the residual birefringence of the substrate. Since the substrate loading in the experiment was close to that of a photomask in a typical exposure tool, this supports the conclusion that stress birefringence is negligible compared to substrate residual birefringence.

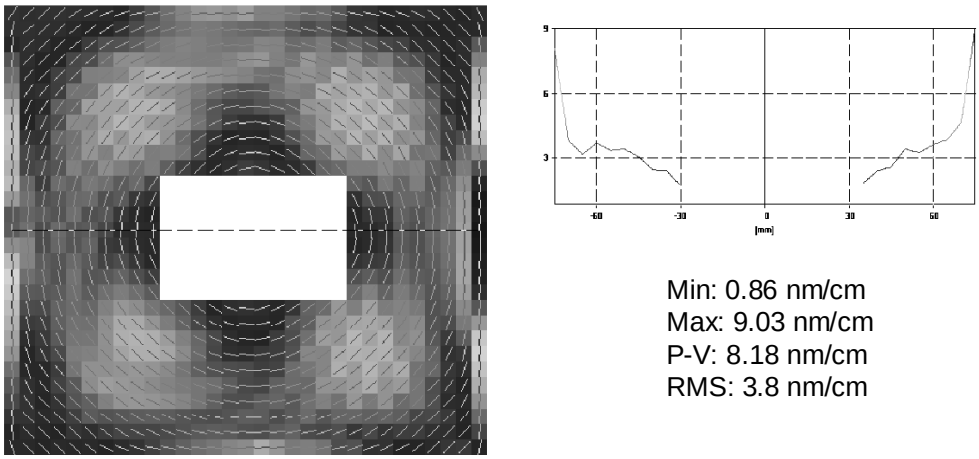

Fig. 10. Experimentally measured birefringence for a substrate under gravity, with an additional 3 kg load in its center.

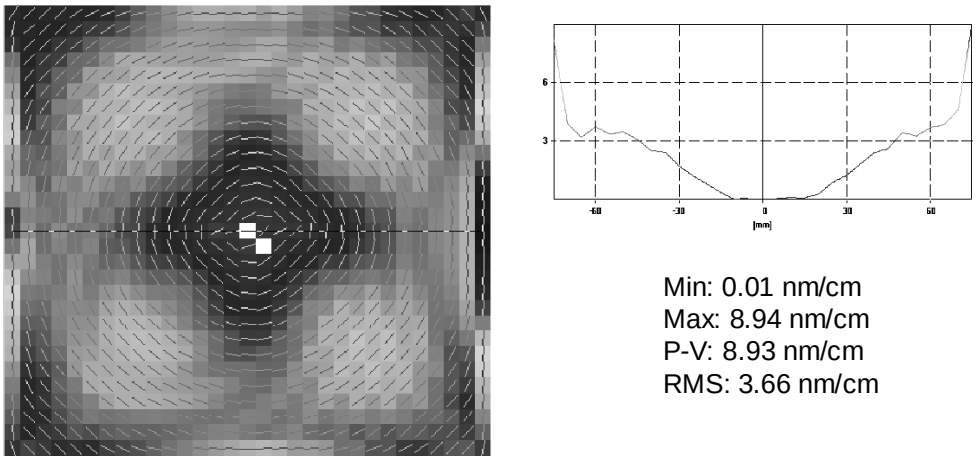

Fig. 11. Experimentally measured birefringence for a substrate under gravity, without any additional load (repeated).

Similarly, the simulations for the case of a mask subjected to a 3 kg load in its center predict that gravity or a load placed at the centre of the blank induce a state of bending stress which leads to a negligible stress birefringence, as shown in Fig. 12. The maximum magnitude of birefringence is 0.55 nm/cm. It must be noted that the arrows in the plot of Fig. 12 are not to be considered as vectors, since birefringence does not have a sign, but are simply meant to represent the orientation of the fast axis at each point.

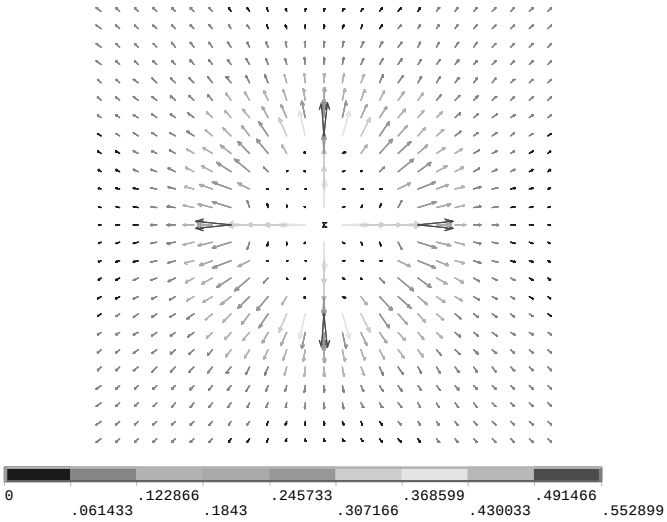

Fig. 12. Numerical results for a 3 kg load placed in the center of a substrate supported on its 4 edges. Scale in nm/cm. Maximum stress birefringence is 0.55 nm/cm.

5. SUMMARY AND CONCLUSIONS

A numerical method for the calculation of stress birefringence in mask substrates was exposed, based on stress-optic relations and Jones calculus. This technique, applied analytically to the case of a mask in a state of uniaxial bending, demonstrated that no stress birefringence was induced by this type of loading, which agreed with the numerical predictions. Further FE simulations were run for loadings corresponding to photomasks with stressed layers, initially non-flat substrates, different pellicles attached to them and being vacuum-chucked in various exposure tools. Different exposure tool mounts were modeled by chucking masks over areas of different sizes and with different pressures. The calculated stress birefringence was in all cases below 1 nm/cm, i.e., negligible compared to specifications. An experiment was performed to verify this in conditions approaching those of a mask in an exposure tool and confirmed that the corresponding bending loads induced no change in birefringence from its initial state. It follows from the analytically and experimentally verified numerical models that no high levels of stress birefringence occur for blanks or masks held in exposure tools. Therefore, the only type of birefringence to monitor is the residual birefringence due to the internal stresses that occur in the photomask substrate during its fabrication.

ACKNOWLEDGMENTS

The first author would like to thank Michael Albert of ASML for his help with Jones calculus, as well as Andrew Grenville and Chris Van Peski of International SEMATECH for their encouragement. AMTC is a joint venture of Infineon, AMD and DuPont Photomasks and gratefully acknowledges the financial support of the German Federal Ministry of Education and Research (BMBF) under contract No. 01M3154A (“Abbildungsmethodiken für nanoelektrische Bauelemente”).

REFERENCES

1. International Technology Roadmap for Semiconductors, 2004 edition, http://public.itrs.net
2. A. R. Mikkelson, M. A. Sprague, R. L. Engelstad, E. G. Lovell, and D. Trost, “Mechanical distortions in advanced optical reticles,” BACUS Symposium on Photomask Technology and Management, SPIE Vol. 3331, pp. 601-611, 1998.

3. A. R. Mikkelson, R. L. Engelstad, M. Mason, and R. S. Mackay, “Effect of chrome stress on pattern transfer mechanical distortions,” Proceedings of the 157 nm Lithography Symposium, 2000.
4. A. R. Mikkelson, A. Y. Amr, E. P. Cotte, J. Sohn, R. L. Engelstad, and E. G. Lovell, “Mask-related distortions of modified fused silica reticles for 157-nm lithography,” BACUS Symposium on Photomask Technology and Management, SPIE Vol. 4562, pp. 914-925, 2001.
5. A. R. Mikkelson, R. L. Engelstad, and E. G. Lovell, “Mechanical distortions in advanced photomasks,” BACUS Symposium on Photomask Technology and Management, SPIE Vol. 3546, pp. 413-421, 1998.
6. K. B. Doyle and W. M. Bell, “Thermo-elastic wavefront and polarization error analysis of a telecommunication optical circulator,” Current developments in lens design and optical systems engineering, SPIE Vol. 4093, pp. 18-27, 2000.
7. K. B. Doyle, J. M. Hoffman, V. L. Genberg, and G. J. Michels, “Stress birefringence modelling for lens design and photonics,“ International optical design conference, SPIE Vol. 4832, pp. 436-447, 2002.
8. K. B. Doyle, V. L. Genberg, and G. J. Michels, “Numerical methods to compute optical errors due to stress birefringence,“ Optical design and analysis software II, SPIE Vol. 4769, pp. 34-42, 2002.
9. V. L. Genberg, K. B. Doyle, and G. J. Michels, “Optical performance as a function of dynamic mechanical loading,“ Optical modelling and performance predictions, SPIE Vol. 5178, pp. 14-19, 2002.
10. V. L. Genberg, G. Michels, K. B. Doyle, “Making FEA results useful in optical design,“ Optical design and analysis software II, SPIE Vol. 4769, pp. 24-33, 2002.
11. A. C. Ugural, *Stresses in plates and shells*, 2nd ed., McGraw-Hill, 1999.
12. *American Institute of Physics Handbook*, 2nd ed., McGraw-Hill, 1963.
13. Y. C. Yiu and A. R. Meyer, “Computation of optical errors in transparent optical elements due to three-dimensional photoelastic effect,“ SPIE Vol. 1303, 1990.
14. R. Priestley, “Birefringence dispersion in photomask substrates for DUV lithography,” BACUS Symposium on Photomask Technology, SPIE Vol. 3873, pp. 587-591, 1999.
15. E. P. Cotte, R. Hässler, B. Utess, G. Antesberger, and F. Kromer, “Pellicle choice for 193-nm immersion lithography photomasks,” BACUS Symposium on Photomask Technology, SPIE Vol. 5567, pp. 511-520, 2004.
16. G. G. Stoney, Proceedings of the Royal Society of London, A82, pp. 172-177, 1909.
17. B. Wang, “Residual birefringence in photomask substrates,” Journal of Microlithography, Microfabrication, and Microsystems, Vol. 1, pp. 43-48, April 2002.
18. B. Wang, C. O. Griffiths, R. R. Rockwell, J. List, and D. Mark, “The exicor DUV birefringence measurement system and its application to measuring lithography-grade CaF2 lens blanks,” Optical diagnostic methods for inorganic materials III, SPIE Vol. 5192, pp. 7-18, 2003.
19. B. Wang and P. M. Troccolo, “Measurement of residual birefringence in photomask blanks,” BACUS Symposium on Photomask Technology, SPIE Vol. 3873, pp. 544-553, 1999.